Acta Oceanol. Sin., 2020, Vol. 39, No. 12, P. 114–120
https://doi.org/10.1007/s13131-020-1687-9
http://www.hyxb.org.cn
E-mail: hyxbe@263.net

Wind speed inversion and in-orbit assessment of the imaging altimeter on Tiangong-2 space station

Youguang Zhang[1, 2], Qingliu Bao[3]*, Mingsen Lin[1], Shuyan Lang[1]

[1] Key Laboratory of Space Ocean Remote Sensing and Application, National Satellite Ocean Application Service, Beijing 100081, China

[2] Southern Marine Science and Engineering Guangdong Laboratory (Guangzhou), Guangzhou 511458, China

[3] Beijing Piesat Information Technology Co., Ltd., Beijing 100195, China

Received 1 July 2019; accepted 17 December 2019

Abstract

Imaging altimeter (IALT) is a new type of radar altimeter system. In contrast to the conventional nadir-looking altimeters, such as HY-2A altimeter, Jason-1/2, and TOPEX/Poseidon, IALT observes the earth surface at low incident angles (2.5°–8°), so its swath is much wider and its spatial resolution is much higher than the previous altimeters. This paper presents a wind speed inversion method for the recently launched IALT onboard Tiangong-2 space station. Since the current calibration results of IALT do not agree well with the well-known wind geophysical model function at low incidence angles, a neural network is used to retrieve the ocean surface wind speed in this study. The wind speed inversion accuracy is evaluated by comparing with the ECMWF reanalysis wind speed, buoy wind speed, and *in-situ* ship measurements. The results show that the retrieved wind speed bias is about –0.21 m/s, and the root-mean-square (RMS) error is about 1.85 m/s. The wind speed accuracy of IALT meets the performance requirement.

Key words: imaging altimeter, ocean surface wind speed, inversion accuracy analysis, in-orbit assessment

Citation: Zhang Youguang, Bao Qingliu, Lin Mingsen, Lang Shuyan. 2020. Wind speed inversion and in-orbit assessment of the imaging altimeter on Tiangong-2 space station. Acta Oceanologica Sinica, 39(12): 114–120, doi: 10.1007/s13131-020-1687-9

1 Introduction

Ocean surface wind field, significant wave height, sea surface current, and sea temperature are important marine dynamical parameters. They play important roles in the monitoring of ocean environment, the forecasting of marine disaster, as well as the maintaining of maritime rights and interests. A synchronous observation of the ocean dynamical parameters is of particular importance to the overall analysis of oceanic dynamic process. Satellite remote sensing is one of the most effective techniques for acquiring the global ocean dynamic parameters. Specifically, microwave remote sensing can be used to observe the ocean at all-weather and all-time conditions. There is a variety of microwave remote sensing payloads that are operated by different communities at present, such as radar altimeters, microwave scatterometers, and microwave radiometers. Different payloads are designed for observing different ocean dynamical parameters, among which the radar altimeters are one of the most widely used microwave remote sensing payloads for monitoring sea surface height, winds, and waves.

Imaging altimeter (IALT) is a new generation of radar altimeter system, which combines the advantages of the interferometric radar altimeter and the synthetic aperture radar (SAR) together. It aims at providing the information of oceanic topography at an accuracy of several centimeters, as well as the information of land topography at an accuracy of several meters (Zhang et al., 2007). The swath of IALT is wide and the spatial resolution of IALT is high. The first IALT onboard Tiangong-2 space station was launched successfully from Jiuquan Satellite Launch Center on September 15, 2016. The in-orbit assessment of IALT was done before April 30, 2017.

In this paper, Section 2 has a brief overview of the IALT system onboard Tiangong-2 space station. Section 3 presents the inversion method of sea surface wind speed. A flowchart is illustrated to describe the overall inversion procedure. The retrieved wind speeds are compared with the European Center for Medium Weather Forecasting (ECMWF) reanalysis wind speed, the buoys wind speed, and the in-site ship measurements. The accuracy of retrieved IALT wind speed is analyzed in Section 4. Finally, the conclusions are addressed in Section 5.

2 IALT on Tiangong-2

IALT is a Ku band interferometric synthetic aperture radar. It was developed by the National Space Science Center, Chinese Academy of Sciences (NSSC). Similar to the traditional real-aperture altimeters, IALT can be used to measure the sea surface height (Bao et al., 2015), the significant wave height (Fan et al., 2014), and sea surface wind speed (Xu et al., 2014). More interestingly, IALT is able to provide the sea wave directional spectrum within a wide swath. The main characteristics of IALT onboard Tiangong-2 space station are summarized in Table 1.

Foundation item: The National Key Research and Development Program of China under contract No. 2016YFC1401002; the Key Special Project for Introduced Talents Team of Southern Marine Science and Engineering Guangdong Laboratory (Guangzhou) under contract No. GML2019ZD0302; the National Natural Science Foundation of China under contract No. 41606202.
*Corresponding author, E-mail: baoqingliu@piesat.cn

Figure 1 shows a photograph of the Tiangong-2 space station docked with the Shenzhou-11 spaceship. The photo was taken by the companion visible light camera on October 23, 2016. Red arrows indicate the antennas of IALT.

3 Wind speed inversion

3.1 *Theoretical geophysical model function (GMF)*

At low incidence angle, the microwave backscattering mechanism over sea surface is dominated by the quasi-specular reflection from small facets oriented perpendicular to the radar look direction. The magnitude of the scattered signal is proportional to the fraction of appropriately oriented facets on the illuminated portion of the sea surface (Cox and Munk, 1954; Barrick, 1974). The theoretical model of microwave backscatter at small incidence angles has been reviewed and analyzed by Brown (1990) and Apel (1994). The normalized radar cross section σ_0 is proportional to the probability density function of the short waves forced by the wind stress. Let $p_s\left(\xi_x, \xi_y\right)$ denotes the joint probability density of the slopes of the facets in two orthogonal horizontal directions, then $p_s\left(-\tan\theta, 0\right)$ corresponds to the fraction of the facets oriented perpendicular to the line connecting the observer and the surface. The backscatter cross section can be written as follow (Freilich and Vanhoff, 2003):

$$\sigma_0\left(\theta\right) = \pi\left|R\left(0\right)\right|^2\left(\sec^4\theta\right)p_s\left(-\tan\theta, 0\right), \tag{1}$$

where σ_0 is the normalized cross section (NRCS) in natural unit, θ is the incidence angle, $\left|R\left(0\right)\right|^2$ is the effective nadir reflection coefficient. This equation is considered to be of sufficient accuracy for the microwave scattering from the ocean at $0° \leqslant \theta \leqslant 15°$ (Valenzuela, 1978; Holliday et al., 1986). Assuming that the sea surface slope is a Gaussian, isotropic random process, Eq. (1) becomes

$$\sigma_0 = \frac{\left|R\left(0\right)\right|^2}{s\left(u\right)}\left(\sec^4\theta\right)\exp\left[\frac{-\tan^2\theta}{s\left(u\right)}\right], \tag{2}$$

where u is the wind speed, and $s\left(u\right)$ is the effective mean square slope. The σ_0 versus incidence angle for different wind speed is shown in Fig. 2.

According to the theory as well as the experiments, the sea surface cross section at low incident angle is not very sensitive to the wind speed, especially at the incidence angle of 10° (Li et al., 2004; Hesany et al., 2004). The quasi-specular reflection dominates the radar backscattering near nadir, thus the NRCS decreases as the wind speed increases. However at medium incidence angles, the Bragg scattering is the dominant factor, thus the NRCS increases as the wind speed increases. The curves of NRCS versus incidence angle for different wind speeds intersects at around 10° (Fig. 2), which means that different wind speeds correspond to the same NRCS at this particular incidence angle. Generally, the derivative of NRCS (versus the incident angle) is used in the wind speed inversion.

Freilich and Vanhoff (2003) compared the model function of the Precipitation Radar (PR) with the least square fitting results at certain selected wind speed (see Fig. 5 in Freilich and Vanhoff, 2003), and found that Eq. (2) does not fit the PR NRCS very well, especially at the low wind speed and high incident angle. Thus, it is necessary to develop an empirical GMF model for the wind speed inversion.

Table 1. The main characteristics of IALT onboard Tiangong-2

Orbit parameters	
Altitude/km	378.6
Velocity/km·s^{-1}	7.3
System parameters	
Polarization	VV
Carrier frequency/GHz	13.58
Peak power/W	300
Baseline/m	2.3
Band width/MHz	40
Incident angle/(°)	2.5–8
Swath/km	30
Spatial resolution/m	20–60

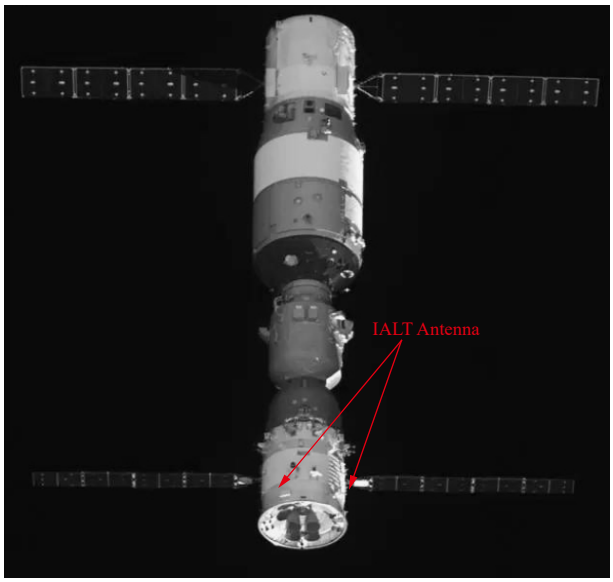

Fig. 1. A photograph of the Tiangong-2 space station docked with the Shenzhou-11 spaceship.

3.2 *Empirical GMF*

For low-incidence observation radar such as the PR on tropic-

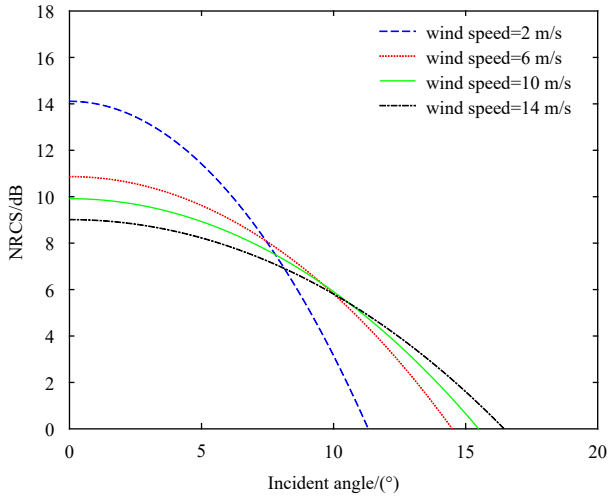

Fig. 2. The NRCS versus incident angle.

al rainfall measuring mission (TRMM) (Kozu et al., 2001), the ocean surface wind speed is usually retrieved by the maximum likelihood estimation (MLE) based on multi-incidence angles (Bao et al., 2016a, b). The accuracy of the MLE-based wind speed inversion is directly determined by the GMF. In order to improve the wind speed retrieval accuracy, a more accurate empirical GMF is established. The empirical GMF is developed by collocating the PR NRCS with QuikScat (Tsai et al., 2000) wind speed data. Here, we use the QuikScat wind speed and PR NRCS data from January 2007 to December 2008 to establish the empirical GMF model. The temporal window and spatial window for the collocation is 10 min and 25 km, respectively.

The established empirical GMF is a two-dimensional look up table, as shown in Fig. 3. The wind speed interval is 0.2 m/s, and the incidence angle interval is 0.8° (determined by the incidence resolution of PR). Figure 3 illustrates the NRCS as a function of wind speed and incident angle, for wind speed lower than 20 m/s and incident angle smaller than 13°. The comparison of theoretical and empirical GMF models at selected wind speeds is shown in Fig. 4. In the wind speed inversion process of IALT, the empirical GMF is used as a reference for quality control in order to remove the abnormal data, such as land and rain contamination (Lin et al., 2014, 2015).

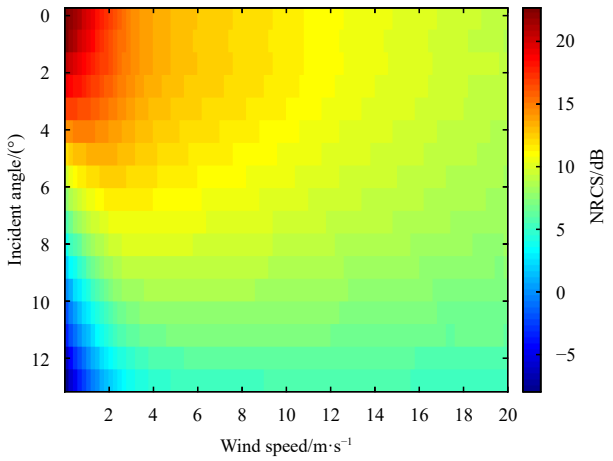

Fig. 3. The empirical GMF of sea surface NRCS at low incidence.

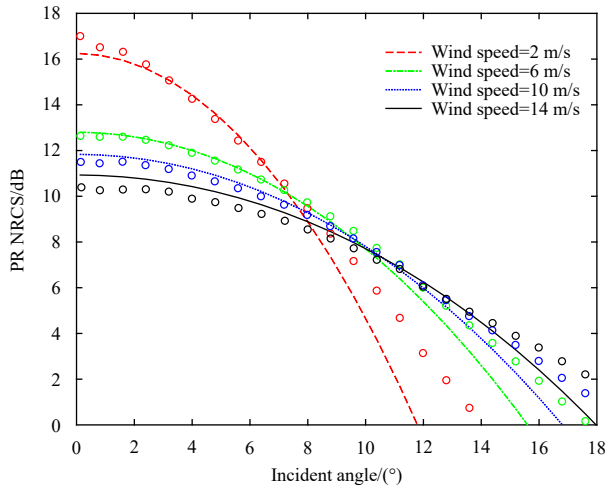

Fig. 4. The comparison of theoretical (line) and empirical (circles) GMF models at selected wind speeds.

3.3 *External calibration*

For the IALT data, the antenna pattern is calibrated using the NRCS of Amazon rain forest in different incident angles. The calibration map of Amazon rain forest at low incident angle is calculated by averaging the TRMM PR data during 2003–2010. The spatial resolution and the incidence resolution of the calibration map are 5 km×5 km and 0.8°, respectively. As an example, Fig. 5 shows the calibration map of Amazon rain forest at θ=7.2°. The absolute NRCS of IALT are acquired after the external calibration.

By statistical calculation, we acquire the sea surface NRCS for different incidence angles, and then compare them with the empirical GMF as shown in Section 3.2. The comparison results for the wind speed of 10 m/s are illustrated in Fig. 6. It is clear that the sea surface NRCS measured by IALT is slightly different from the empirical GMF, which difference is typically smaller than 0.3 dB.

3.4 *Inversion flowchart*

Due to the inaccurate absolute calibration of the antenna gain pattern, the IALT NRCS is slightly different from the GMF, and in turn, both the theoretical and the empirical GMF models are not suitable for IALT wind speed inversion. Thus, we use the neural network algorithm to retrieve the sea surface wind speed for IALT. The wind speed inversion flowchart is shown in Fig. 7.

Firstly, the NRCS data of IALT are obtained by preprocessing the data with the real aperture mode. The sea surface NRCS are

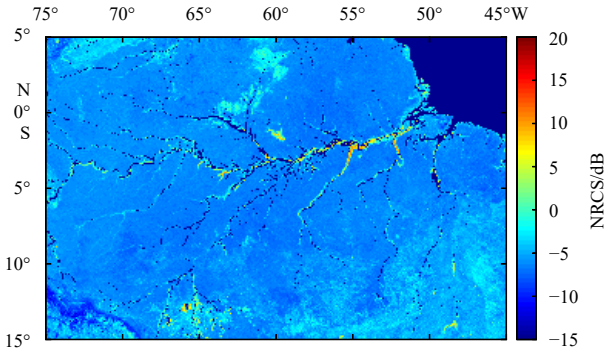

Fig. 5. Amazon rain forest calibration map for NRCS (incident angle: 7.2°).

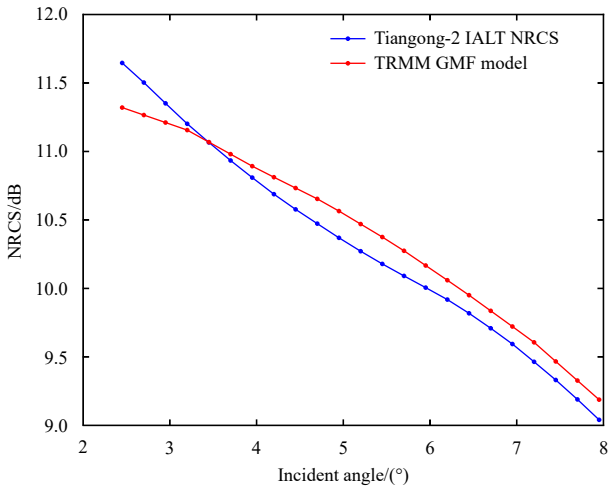

Fig. 6. The comparison of IALT NRCS and empirical GMF model at wind speed of 10 m/s.

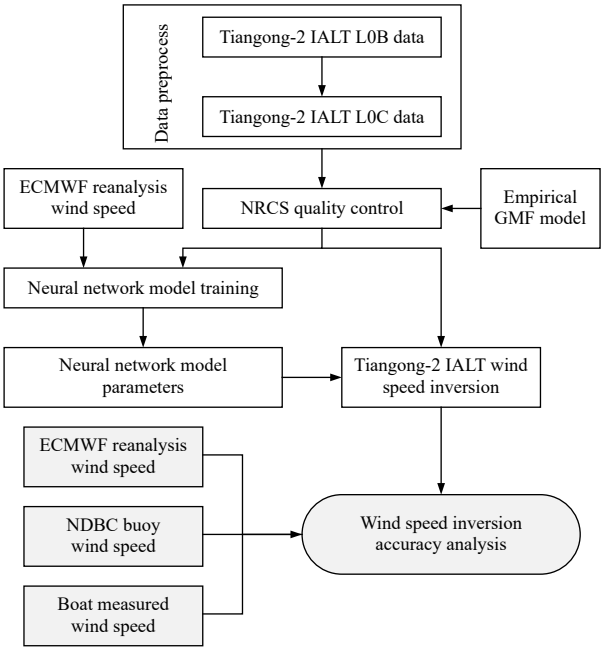

Fig. 7. Flowchart of the wind speed inversion and accuracy analysis for IALT. NDBC represents the National Data Buoy Center.

averaged in both along-track and cross-track directions. The spatial window for the along-track average is 25 km, and the incidence angle window for the cross-track average is 0.25°. Secondly, the NRCS data are evaluated by quality control. The empirical GMF model introduced in Section 3.2 is used as a reference to define the quality of the IALT NRCS data. Thirdly, a neural network is applied to train the model parameters. Part of the quality-controlled IALT NRCS data are collocated with the ECMWF reanalysis wind speed data, and then are used as the training samples. The model parameters obtained by neural network algorithm are consequently used in the IALT wind speed inversion. Finally, the inversion accuracies are analyzed by the ECMWF, National Data Buoy Center (NDBC) buoy, and *in-situ* measurements. The inversion results of IALT at Eastern Pacific Ocean and the adjacent sea areas of China (in December 2016) are shown in Fig. 8.

4 In-Orbit assessment

4.1 *Assessment with the ECMWF reanalysis wind speed*

The ECMWF reanalysis wind speed data (ERA-Interim) are used in the assessment. Its spatial resolution and temporal resolution are 0.25°×0.25° and 6 h respectively. The collocated ERA-Interim and IALT data are acquired by spatially and temporally interpolating the ECMWF reanalysis data to the IALT acquisitions. First, the wind cells of IALT are partitioned to a size of 25 km× 25 km. Then the central position and the UTC time of IALT wind cells are derived. The ECMWF reanalysis data is actually interpolated spatially and temporally to the above geolocation and observing time.

Practically, the IALT NRCS data and the collocated ECMWF reanalysis wind speeds on the first half of December 2016 are used as the training samples. The wind speed inversion model of IALT is trained by the neural network algorithm. There are 2 631 samples used in the training. We use a two-layer feed-forward network with sigmoid hidden neurons (25) and linear output neurons. The network is trained with Levenberg-Marquardt backpropagation algorithm. The schematic diagram of the two-layer feed-forward network is shown in Fig. 9.

Using the wind speed inversion model trained by neural network algorithm, the IALT NRCS data from second half of December 2016 to January 2017 are retrieved. The retrieved wind speeds are compared with the ECMWF reanalysis wind speeds, and the wind speed inversion accuracy is analyzed. Figure 10 shows the scatter plot of the retrieved wind speed versus ECMWF winds. Black line indicates the correspondence along the diagonal. There are 5 848 wind cells in total. Comparing with the ECMWF reanalysis wind speeds, the IALT retrieved wind speeds have a negative bias of 0.21 m/s, a root mean square (RMS) of 1.85 m/s, and a correlation coefficient of 0.78. Basically, the IALT wind speed accuracy meets its specification, which requires that the RMS error of wind speed should be smaller than 2 m/s.

4.2 *Assessment with the NDBC buoy wind speed*

The buoys of NDBC meteorological/ocean program belong to the NDBC. They mostly locate near the east and the west coast of United State. The NDBC buoys have different types. The anemometers are installed on different heights depending on the sizes of the platforms. For the sake of comparison, the wind speeds

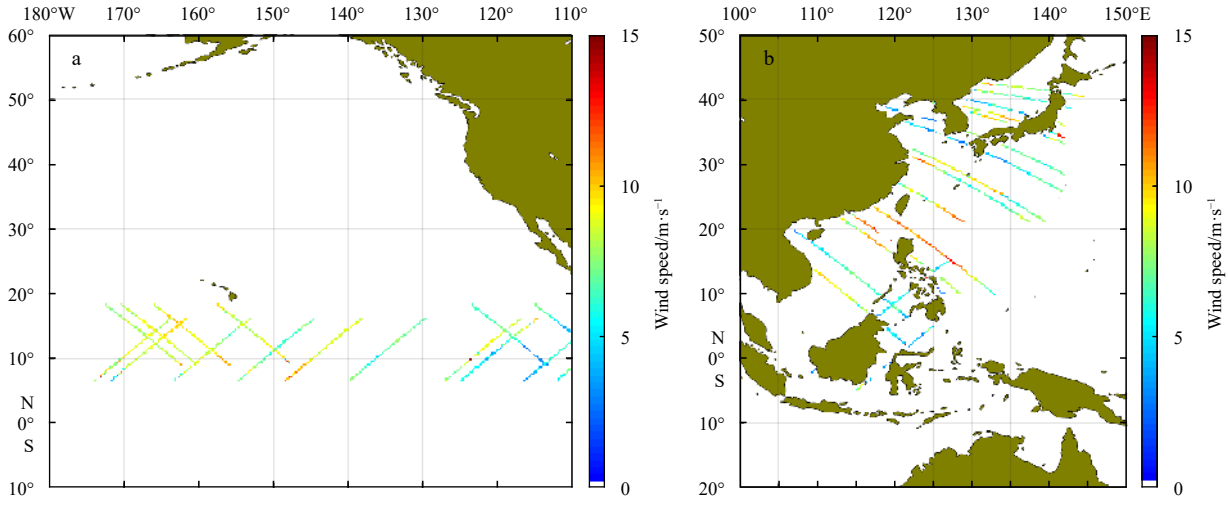

Fig. 8. The wind speed inversion results of IALT. a. Eastern Pacific Ocean, b. the adjacent sea areas of China.

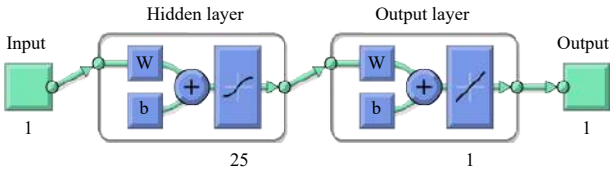

Fig. 9. Training diagram of the wind speed inversion model.

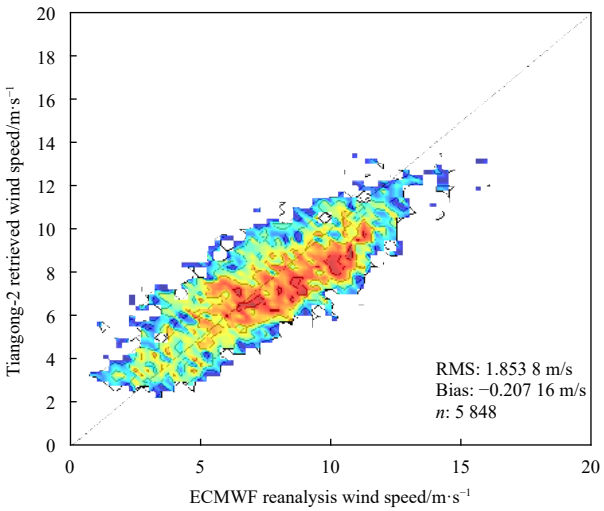

Fig. 10. The scatter diagram of IALT wind speed inversion.

measured by NDBC buoy are also converted to 10 m equivalent neutral stability wind speed. In this paper, we use three buoys (51000, 51004, 51101) that locate over the open sea (near Hawaii) to validate the retrieved wind speeds. The positions of these NDBC buoys are illustrated in Fig. 11.

Moreover, the buoy data with high temporal resolution (10 min) are used. Consequently, the IALT retrieved wind speed can be collocated with the buoy data using a temporal window of ±5 min. To acquire as many buoy collocations as possible, the spatial window of IALT-buoy collocations is set to 50 km. Finally, the IALT data from December 2016 to March 2017 are used, and 15 matchup samples with the buoys are obtained, as shown in Table 2. The rightmost column of Table 2 indicates that all of the

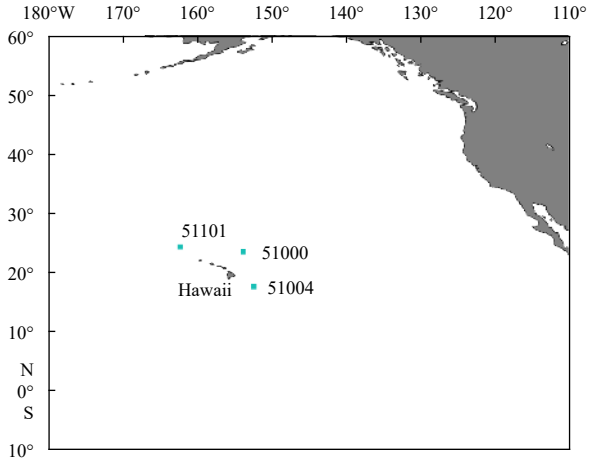

Fig. 11. The position of NDBC buoys.

wind speed differences are within ±2 m/s. The retrieved wind speeds have a mean bias of 0.144 m/s and a RMS of 1.32 m/s.

4.3 *Assessment with the ship measurements*

In March 2017, the National Satellite Ocean Application Service (NSOAS) carried out several *in-situ* measurements on the south of Hainan Island in order to verify the observation accuracy of IALT on Tiangong-2 space station. The *in-situ* wind speeds were measured on March 16, 19, and 22 respectively. The ship positions, the actual wind speed, and the retrieved wind speed are shown in Fig. 12. The comparison with ship measurements are presented in Table 3.

Note that the positions of *in-situ* measurements are nearshore, which is primarily designed to validate the sea surface height measurements of IALT. From Table 3 we know that the wind speed difference on March 22 is about 2.9 m/s, and the wind speed differences on March 16 and 19 are smaller than ±2 m/s. The main objective of TB03 measurements is to validate the ocean color retrieved from the Multi-angle wide band imager on Tiangong-2, such that TB03 is about 10 km offshore, which is much closer to coast than TB01 and TB02. This may be the main reason that the estimation error at TB03 is quite larger than that at TB01 and TB02.

Table 2. The comparison of IALT retrieved wind speeds with buoy wind speeds

Buoy No.	UTC time	IALT wind speed/m·s^{-1}	Buoy wind speed/m·s^{-1}	Wind speed difference/m·s^{-1}
51000	2016/12/04 12:26:35.4	11.15	9.8	1.35
	2016/12/04 12:26:38.9	10.89	9.8	1.09
	2016/12/04 12:26:42.3	11.78	9.8	1.98
	2016/12/04 12:26:45.8	11.39	9.8	1.59
	2017/03/19 11:36:46.5	3.63	3.8	−0.17
	2017/03/19 11:36:49.9	4.57	3.8	0.77
	2017/03/19 11:36:53.4	3.60	3.8	−0.2
51004	2016/12/05 11:23:49.4	7.46	6.8	0.66
	2016/12/05 11:23:52.9	5.36	6.8	−1.44
	2016/12/05 11:23:56.3	6.15	6.8	−0.65
	2016/12/16 06:26:15.1	4.58	3.3	1.28
	2016/12/16 06:26:18.5	4.58	3.3	1.28
51101	2017/03/15 14:03:43.9	3.94	5.8	−1.86
	2017/03/15 14:03:47.4	4.03	5.8	−1.77
	2017/03/15 14:03:50.8	4.05	5.8	−1.75

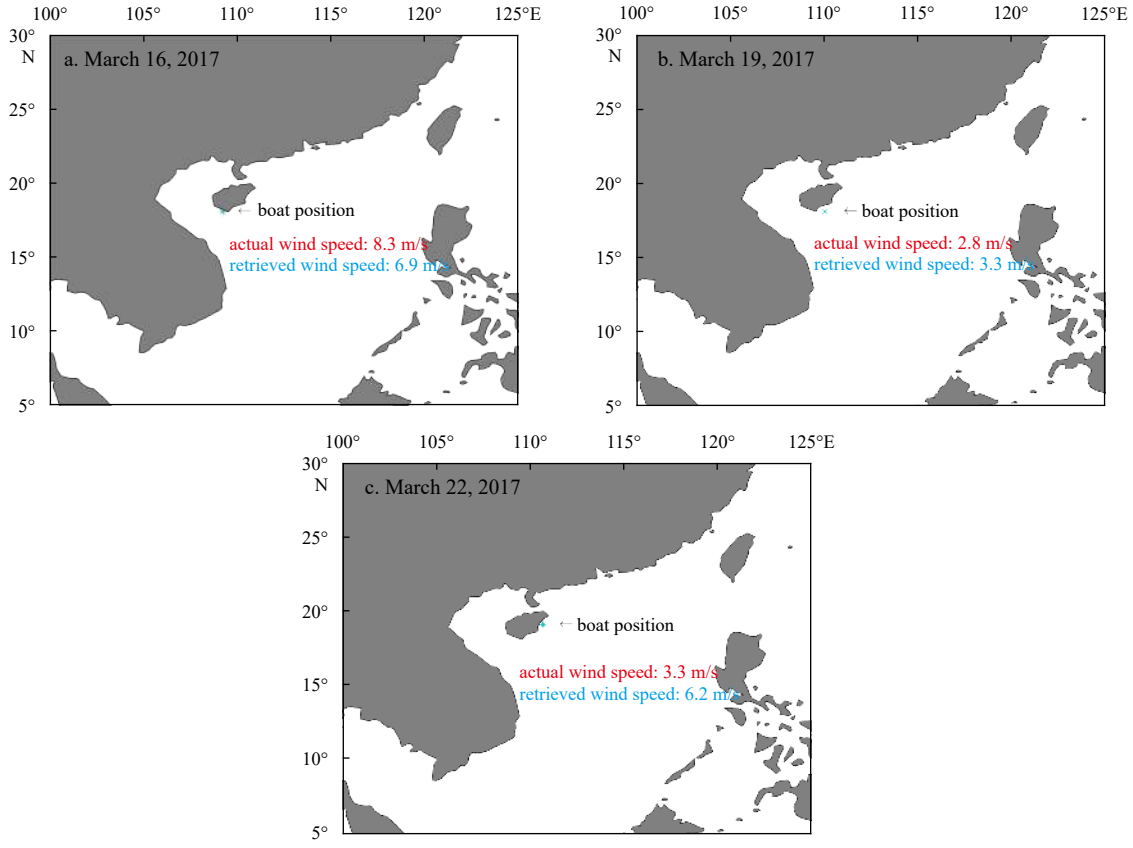

Fig. 12. The *in-situ* wind speed measurements.

Table 3. The comparison of IALT wind speeds and ship measurements

Station No.	North latitude/(°)	East longitude/(°)	Beijing time	IALT wind speed/m·s^{-1}	*In-situ* wind speed/m·s^{-1}	Wind speed difference/m·s^{-1}
TB01	18.101 1	109.235 3	2017/3/16 12:15	6.9	8.3	–1.4
TB02	18.102 6	110.055 4	2017/3/19 10:31	3.3	2.8	0.5
TB03	19.089 4	110.667 2	2017/3/22 09:17	6.2	3.3	2.9

5 Conclusions

IALT is a new generation of radar altimeter system, which operates at Ku band microwave frequency. It can be used to derive the sea surface height, the significant wave height, the sea surface wind speed, and the sea wave directional spectrum simultaneously. Comparing with the traditional radar altimeters such as Jason-2 and HY-2A altimeter, its swath is wider and its spatial resolution is higher.

In this paper, we briefly introduce the IALT radar system on board Tiangong-2 space station. Then a neural network algorithm is used to train the inversion model, and consequently is applied to the wind speed inversion of IALT. In order to assess the accuracy of IALT wind speeds, we compare the retrieved wind speed with the ECMWF, buoy, and *in-situ* measurements. The RMS error of the retrieved wind speed is about 1.85 m/s, and the mean bias is smaller than 0.21 m/s, implying that the accuracy of IALT wind speed satisfies its specification.

Note also that the retrieved wind speeds are lower than the ECMWF reanalysis wind speeds under high wind speed condition (Fig. 10), especially for wind speed larger than 15 m/s. While at low wind speeds, the retrieved wind speeds are a little overestimated. The reasons could be: first, the small amount of training samples limits the wind speed range in neural network algorithm. Second, the quality control is imperfect at present. The future work will focus on the improvement of the wind speed inversion method, as well as the selection of the training samples.

References

Apel J R. 1994. An improved model of the ocean surface wave vector spectrum and its effects on radar backscatter. Journal of Geophysical Research: Oceans, 99(C8): 16269–16291, doi: 10.1029/94JC00846

Bao Lifeng, Gao Peng, Peng Hailong, et al. 2015. First accuracy assessment of the HY-2A altimeter sea surface height observations: cross-calibration results. Advances in Space Research, 55(1): 90–105

Bao Qingliu, Zhang Youguang, An Wentao, et al. 2016a. Sea surface wind speed inversion using low incident NRCS. In: Proceedings of 2016 IEEE International Geoscience and Remote Sensing Symposium (IGARSS). Beijing: IEEE, 4619–4622

Bao Qingliu, Zhang Youguang, Lang Shuyan, et al. 2016b. Sea surface wind speed inversion using the low incident NRCS measured by TRMM precipitation radar. IEEE Journal of Selected Topics in Applied Earth Observations and Remote Sensing, 9(11): 5262–5271, doi: 10.1109/JSTARS.2016.2581215

Barrick D. 1974. Wind dependence of quasi-specular microwave sea scatter. IEEE Transactions on Antennas and Propagation, 22(1): 135–136, doi: 10.1109/TAP.1974.1140736

Brown G S. 1990. Quasi-Specular scattering from the air-sea interface. In: Geernaert G L, Plant W L, eds. Surface Waves and Fluxes. Dordrecht: Springer, 1–39

Cox C, Munk W. 1954. Statistics of the sea surface derived from sun glitter. Journal of Marine Research, 13(2): 198–227

Fan Chenqing, Zhang Jie, Meng Junmin, et al. 2014. Significant wave height operational inversion algorithm of HY-2A altimeter. Haiyang Xuebao (in Chinese), 36(3): 121–126

Freilich M H, Vanhoff B A. 2003. The relationship between winds, surface roughness, and radar backscatter at low incidence angles from TRMM precipitation radar measurements. Journal of Atmospheric and Oceanic Technology, 20(4): 549–562

Hesany V, Plant W J, Keller W C. 2004. The normalized radar cross section of the sea at 10° incidence. IEEE Transactions on Geoscience and Remote Sensing, 38(1): 64–72

Holliday D, St-Cyr G, Woods N E. 1986. A radar ocean imaging model for small to moderate incidence angles. International Journal of Remote Sensing, 7(12): 1809–1834, doi: 10.1080/01431168608948971

Kozu T, Kawanishi T, Kuroiwa H, et al. 2001. Development of precipitation radar onboard the Tropical Rainfall Measuring Mission (TRMM) satellite. IEEE Transactions on Geoscience and Remote Sensing, 39(1): 102–116, doi: 10.1109/36.898669

Li Li, Im E, Connor L N, et al. 2004. Retrieving ocean surface wind speed from the TRMM Precipitation Radar measurements. IEEE Transactions on Geoscience and Remote Sensing, 42(6): 1271–1282, doi: 10.1109/TGRS.2004.828924

Lin Wenming, Portabella M, Stoffelen A, et al. 2014. Rain identification in ASCAT winds using singularity analysis. IEEE Geoscience and Remote Sensing Letters, 11(9): 1519–1523, doi: 10.1109/LGRS.2014.2298095

Lin Wenming, Portabella M, Stoffelen A, et al. 2015. ASCAT wind quality control near rain. IEEE Transactions on Geoscience and Remote Sensing, 53(8): 4165–4177, doi: 10.1109/TGRS.2015.2392372

Tsai W T, Spencer M, Wu C, et al. 2000. SeaWinds on QuikSCAT: sensor description and mission overview. In: Proceedings of IEEE 2000 International Geoscience and Remote Sensing Symposium, Taking the Pulse of the Planet: The Role of Remote Sensing in Managing the Environment. Honolulu: IEEE, 1021–1023

Valenzuela G R. 1978. Theories for the interaction of electromagnetic and oceanic waves: A review. Boundary-Layer Meteorology, 13(1): 61–85

Xu Yuan, Yang Jingsong, Zheng Gang, et al. 2014. Calibration and verification of sea surface wind speed from satellite altimeters. Haiyang Xuebao (in Chinese), 36(7): 125–132

Zhang Yunhua, Zhang Xiangkun, Meng Xin, et al. 2007. An interferometric imaging altimeter applied for both ocean and land observation. In: Proceedings of 2007 IEEE International Geoscience and Remote Sensing Symposium. Barcelona: IEEE, 3821–3824